Modelling current-induced magnetization switching in Heusler alloy Co2FeAl-based spin-valve nanopillar

H. B. Huang, X. Q. Ma, Z. H. Liu, C. P. Zhao, and L. Q. Chen

Articles you may be interested in

001 textured polycrystalline current-perpendicular-to-plane pseudo spin-valves using Co2Fe(Ga0.5Ge0.5) Heusler alloy
Appl. Phys. Lett. **103**, 202401 (2013); 10.1063/1.4829633

Simulation of multilevel cell spin transfer switching in a full-Heusler alloy spin-valve nanopillar
Appl. Phys. Lett. **102**, 042405 (2013); 10.1063/1.4789867

Spin transfer switching characteristics in a [Pd/Co]m/Cu/[Co/Pd]n pseudo spin-valve nanopillar with perpendicular anisotropy
J. Appl. Phys. **111**, 07C910 (2012); 10.1063/1.3675150

Micromagnetic simulation of spin-transfer switching in a full-Heusler Co2FeAl0.5Si0.5 alloy spin-valve nanopillar
J. Appl. Phys. **110**, 033913 (2011); 10.1063/1.3619773

Current-induced magnetic switching in nanopillar spin-valve systems with double free layers
J. Appl. Phys. **101**, 09A512 (2007); 10.1063/1.2714314

Modelling current-induced magnetization switching in Heusler alloy Co$_2$FeAl-based spin-valve nanopillar

H. B. Huang,[1,2] X. Q. Ma,[2] Z. H. Liu,[2] C. P. Zhao,[2] and L. Q. Chen[1]

[1]*Department of Materials Science and Engineering, The Pennsylvania State University, University Park, Pennsylvania 16802, USA*
[2]*Department of Physics, University of Science and Technology Beijing, Beijing 100083, China*

We investigated the current-induced magnetization switching in a Heusler alloy Co$_2$FeAl-based spin-valve nanopillar by using micromagnetic simulations. We demonstrated that the elimination of the intermediate state is originally resulted from the decease of effective magnetic anisotropy constant. The magnetization switching can be achieved at a small current density of 1.0×10^4 A/cm^2 by increasing the demagnetization factors of x and y axes. Based on our simulation, we found magnetic anisotropy and demagnetization energies have different contributions to the magnetization switching. © *2014 AIP Publishing LLC*. [http://dx.doi.org/10.1063/1.4870291]

I. INTRODUCTION

In the past decades, spin transfer torque (STT)[1,2] has attracted considerable attention due to its application in high density magnetic random access memory (MRAM).[3–7] Spin polarized electrons carried spin angular momenta from the fixed layer to the free layer. It causes free layer to switch when the current density exceeds a critical current density J$_c$. However, the critical current density required to induce magnetization switching in the spin-valves is as high as 10^6–10^8 A/cm^2, and it is challenging to reduce J$_c$ to achieve the compatibility with highly scaled complementary metal-oxide-semiconductor technology while maintaining thermal stability.[8–12] Recently, Heusler alloys[13] with lower saturation magnetization M$_s$, smaller Gilbert damping constant α, and higher spin polarization constant η are demonstrated to be excellent candidates for reducing J$_c$ compared to the normal metal and metallic alloys, i.e., Fe,[14,15] Co,[16–18] CoFe,[19,20] Py,[21–23] and CoFeB.[24–27]

Existing experimental work demonstrated that J$_c$ of Co$_2$MnGe, Co$_2$FeSi, and Co$_{75}$Fe$_{25}$ spin-valves were 1.6×10^7, 2.7×10^7, and 5.1×10^7 J/cm^2, respectively.[28] Spin transfer torque switching was also achieved experimentally in Co$_2$FeAl$_{0.5}$Si$_{0.5}$ (CFAS)-based spin valve, exhibiting a two-step magnetization switching.[29] In our previous work, we demonstrated that the two-step switching was resulted from the four-fold magnetic anisotropy of CFAS and asymmetric spin transfer torque.[30] Based on the two-step switching, we continued to develop a multilevel bit spin transfer multi-step magnetization switching by changing the magnetic anisotropy.[31] Recently, Sukegawa *et al.*[32] reported the spin transfer switching of Heusler Co$_2$FeAl (CFA)-based spin valve, where the intermediate state was not found in the current-induced magnetization switching. However, there has been no explanation for the absence of the intermediate state in full-Heusler CFA spin valve nanopillar. Furthermore, the critical current density of 2.9×10^7 A/cm^2 due to the enhancement of the Gilbert damping constant of CFA is too large for the application. Therefore, a theoretical understanding of spin transfer

switching of CFA-based nanopillar is necessary to reduce the critical current density.

In this paper, we investigated the effects of magnetic anisotropy and demagnetization in the spin transfer torque switching of a Heusler alloy CFA-based spin-valve nanopillar by using micromagnetic simulations. We demonstrated that the elimination of the intermediate state results from the decrease of effective magnetic anisotropy constant. In addition, the critical current density of magnetization switching can be reduced to 1.0×10^4 A/cm^2 by increasing the demagnetization factors along x and y axes. We also discussed the effects of magnetic anisotropy and demagnetization fields.

II. MODEL DESCRIPTION

Figure 1(a) shows the geometry of spin-valve CFA (30 nm)/Ag (4 nm)/CFA (2 nm) and the elliptical cross section area is 250×190 nm^2. We employ a Cartesian coordinate system where the x-axis is the long axis of the ellipse along the CFA [110] direction (easy axis) and the y-axis is along the short axis ([$\bar{1}$10]). The two CFA layers are separated by a thin Ag layer, and the bottom CFA layer is the free layer whose magnetization dynamics is triggered by a spin-polarized current. The top CFA layer is the pinned layer with its magnetization vector **P** fixed in the direction along the positive x axis. The initial magnetization vector **M** of the layer is along the negative or positive x axis. The positive current is generally defined as electrons flowing from the pinned layer to the free layer. In this paper, we focus on the effect of the magnetic anisotropy and demagnetization energies on magnetization switching. As shown in Figure 1(b), we observed a four-fold magnetic anisotropy field along x and y axes, and the demagnetization field along x, y, and z axes. Due to the ultrathin film, the thickness of the free layer is much more lesser than its lateral dimensions. The presence of an out-of-plane component of magnetization leads to a large demagnetization field perpendicular to the plane of the layer. This demagnetization field forces the magnetization
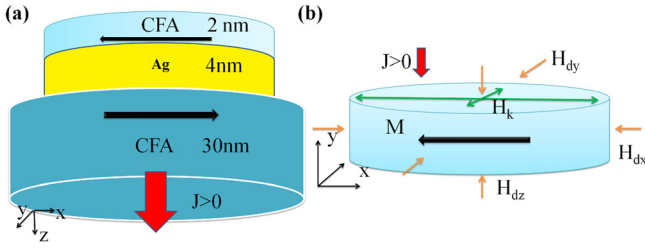
115, 133905-1

FIG. 1. Model geometry definition of CFA-based spin valve in Cartesian coordinates (left). Different contributions of magnetocrystalline anisotropic field $\mathbf{H}_k$, demagnetization field $\mathbf{H}_d$ in the free layer (right).

vector of the free layer to precess along a direction normal to the film plane and impede the magnetization switching.

The magnetization dynamics is described by using a generalized Landau-Lifshitz-Gilbert-Slonczewski (LLGS) equation,[1,2] which can be written as

$$\frac{d\mathbf{M}}{dt} = -\gamma' \mathbf{M} \times \mathbf{H}_{eff} - \frac{\alpha\gamma'}{M_s} \mathbf{M} \times (\mathbf{M} \times \mathbf{H}_{eff})$$
$$- \frac{2\mu_B J}{(1+\alpha^2)edM_s^3} g(\mathbf{M}, \mathbf{P}) \mathbf{M} \times (\mathbf{M} \times \mathbf{P})$$
$$+ \frac{2\mu_B \alpha J}{(1+\alpha^2)edM_s^2} g(\mathbf{M}, \mathbf{P})(\mathbf{M} \times \mathbf{P}), \quad (1)$$

where $\mathbf{H}_{eff}$ is the effective field, $\gamma' = \gamma/(1+\gamma^2)$, γ is the electron gyromagnetic ratio, and α is the dimensionless damping parameter. The effective field includes the magnetocrystalline anisotropy field, the demagnetization field, the external field, and the exchange field, namely $\mathbf{H}_{eff} = \mathbf{H}_k + \mathbf{H}_d + \mathbf{H}_{ext} + \mathbf{H}_{ex}$. In addition, regarding STT term, μ_B, J, d, e, M_s, are the Bohr magneton, the current density, the thickness of the free layer, the electron charge, and the saturation magnetization, respectively. The scalar function[1,2] g(M, P) is given by g(M, P) $= [-4 + (1+\eta)^3(3 + \mathbf{M} \cdot \mathbf{P}/M_s^2)/4\eta^{3/2}]^{-1}$, where the angle between **M** and **P** is θ. $\mathbf{M} \cdot \mathbf{P}/M_s^2 = \cos\theta$.

The magnetic parameters are adopted as followed: saturation magnetization $M_s = 9.0 \times 10^5$ A/m, exchange constant $A = 2.0 \times 10^{-11}$ J/m, Gilbert damping parameter $\alpha = 0.01$, and spin polarization factor $\eta = 0.76$.[29] The initial magnetizations of free and pinned layers are along the $-x$ axis and $+x$ axis, respectively. The dynamics of magnetization was investigated by numerically solving the time-dependent LLGS equation using the Gauss-Seidel projection method[33–36] with a constant time step $\Delta t = 0.0238993$ ps. The samples were discrete in computational cells of $2 \times 2 \times 2$ nm^3.

III. RESULTS AND DISCUSSION

We investigated the effects of magnetic anisotropy and demagnetization fields in current-induced magnetization switching in a full-Heusler CFA-based spin-valve nanopillar of 250×190 nm^2 by using numerical simulations. Figure 2(a) shows the temporal magnetization component evolutions of $\langle m_x \rangle$ at a constant current density of 4.0×10^6 A/cm^2. There are three lines representing magnetization evolutions with different magnetic anisotropy constants: -1.0×10^4 J/m^3 (black), -1.0×10^3 J/m^3 (red), and 2.8×10^3 J/m^3 (blue). In the experiment,[29] three states were obtained: the parallel (P), antiparallel (AP), and intermediate (I: perpendicular to P) states. The intermediate state appears at a constant current density, and the magnetization switching is called 90° switching. We attributed this 90° switching to the balance between STT and the fourfold in-plane magnetocrystalline anisotropy of Heusler-based free layers.[30] The 90° switching (half switching) behavior, as observed experimentally, was obtained at the large magnetic anisotropy constant of -1.0×10^4 J/m^3. However, the intermediate state disappears when the magnetic anisotropy constant K_1 decreases to -1.0×10^3 J/m^3. Therefore, 180° switching can be achieved at the same current due to the decease of the magnetic anisotropy constant. Furthermore, we also observe 180° magnetization switching under the positive magnetic anisotropy constant of 2.8×10^3 J/m^3. It is concluded that the elimination of 90° switching is resulted from the decrease of
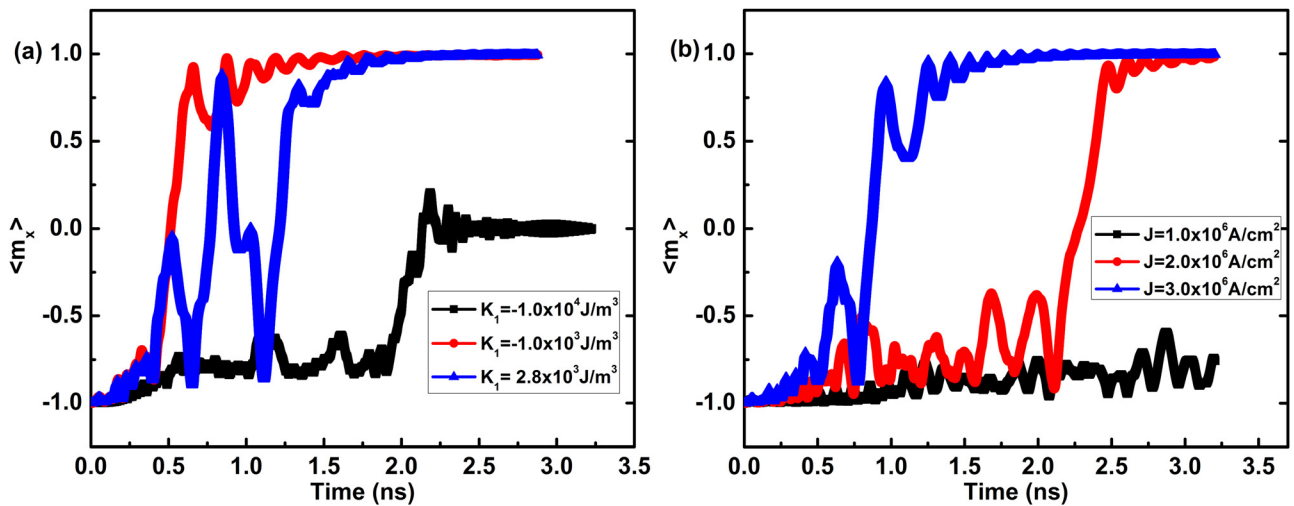

FIG. 2. (a) The temporal magnetization component evolutions of $\langle m_x \rangle$ at the constant current density of 4.0×10^6 A/cm^2 with different magnetic anisotropy constants of -1.0×10^4 J/m^3 (black), -1.0×10^3 J/m^3 (red), and 2.8×10^3 J/m^3 (blue). (b) The temporal magnetization component evolutions of $\langle m_x \rangle$ with different current densities of 1.0×10^6 A/cm^2 (black), 2.0×10^6 A/cm^2 (red), and 3.0×10^6 A/cm^2 (blue) at the same magnetic anisotropy constant of 2.8×10^3 J/m^3.
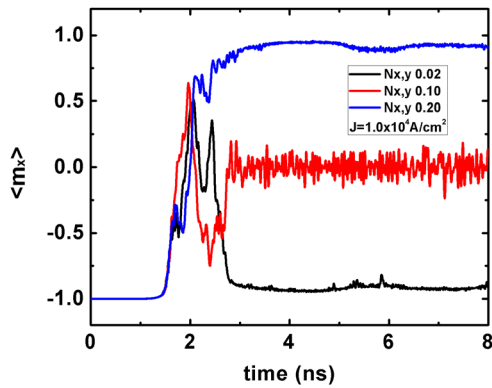
FIG. 3. The temporal magnetization component evolutions of $\langle m_x \rangle$ at the constant current density of $1.0 \times 10^4 \, \text{A/cm}^2$ with different demagnetization factors $N_{x,y}$.

effective magnetic anisotropy constant $|K_1|$. Figure 2(b) shows the temporal magnetization component evolutions of $\langle m_x \rangle$ at the same magnetic anisotropy constant of $2.8 \times 10^3 \, \text{J/m}^3$. There are three lines representing magnetization evolutions with different current densities: $1.0 \times 10^6 \, \text{A/cm}^2$ (black), $2.0 \times 10^6 \, \text{A/cm}^2$ (red), and $3.0 \times 10^6 \, \text{A/cm}^2$ (blue). It is observed that there is no 90° switching in the magnetization switching with the increase of current density. Therefore, we provide the evidence for the elimination of the intermediate state in full-Heusler CFA-based spin valve.

Figure 3 shows the temporal magnetization component evolutions with different demagnetization factors $N_{x,y}$ ($N_x = N_y$). The magnetization is driven by a small current density of $1.0 \times 10^4 \, \text{A/cm}^2$. Magnetization switching cannot

be accomplished if the demagnetization factors N_x and N_y are equal to 0.02. However, we observe 90° and 180° magnetization switching at a small current density of $1.0 \times 10^4 \, \text{A/cm}^2$ when N_x ($N_x = N_y$) increases to 0.10 and 0.20, respectively. In our simulation, the size of the free layer in z direction (2 nm) is significantly smaller than those of x and y directions (250 nm × 190 nm), resulting in much stronger demagnetization fields in z direction. The higher demagnetization field in z direction impedes the development of $\langle m_z \rangle$. Therefore, the demagnetization field along z axis is a barrier prohibiting the magnetization switching from the initial −x direction to the final x direction. However, by decreasing the z axis demagnetization factor and increasing the x or y axe demagnetization factors, the magnetization can be switched easily at a small current. This provides an effective method to decrease the critical current density of spin transfer switching of CFA-based nanopillar.

As shown in Figure 4, the corresponding magnetization distributions of the $250 \times 190 \text{ nm}^2$ ellipse under different demagnetization factors present different magnetization switching behavior. The colors represent different domain area, orange −x, yellow +x, green +y axis, and dark green −y axis, respectively. In the first row, the initial magnetization is along −x axis with a single domain at 1.195 ps. After applying a constant current density of $1.0 \times 10^4 \, \text{A/cm}^2$, the multi-domain could be found at 1.673 ns. The magnetization will become the single domain along −x axis again since STT input energy can overcome the energy barrier. This multi-domain evolution process can be explained by the large current input energy. The energy per unit time pumped into the nanopillar by the current is so large that the
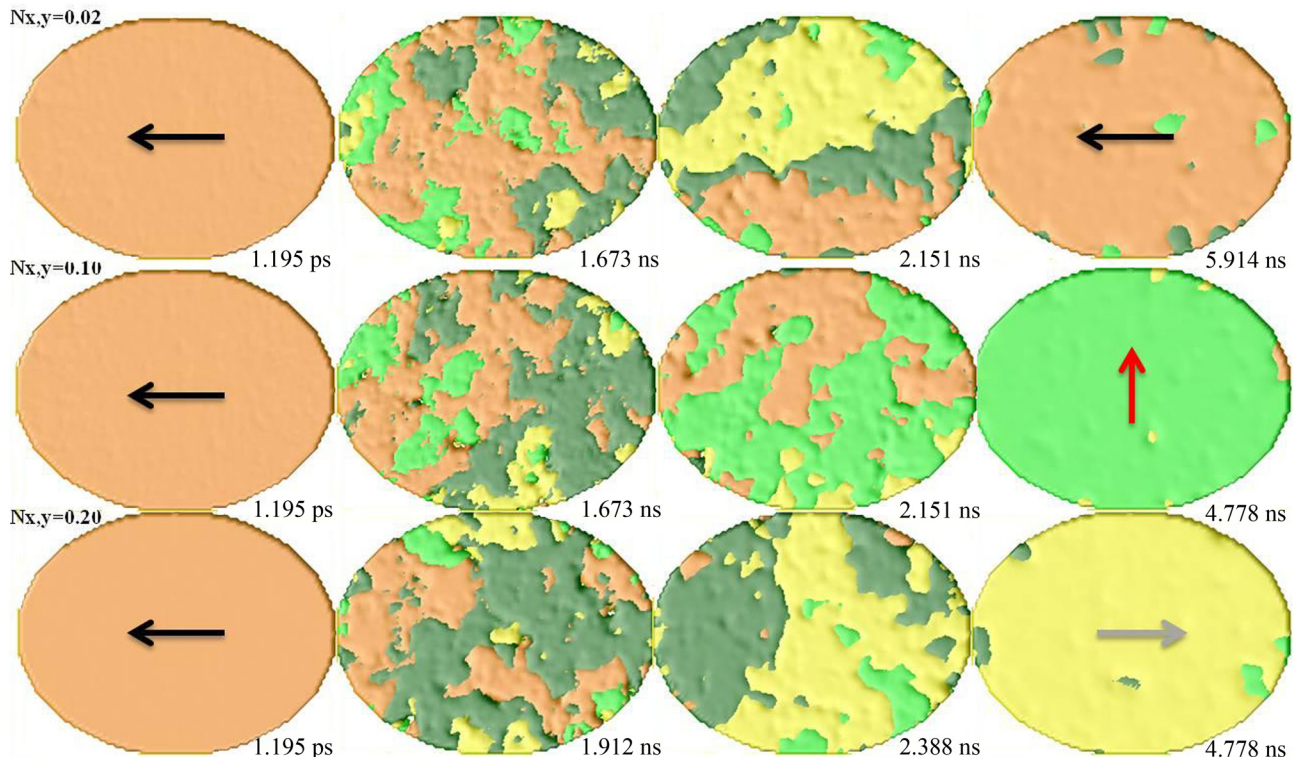

FIG. 4. Snapshots of magnetization distribution of the $250 \times 190 \text{ nm}^2$ ellipse under different demagnetization factors. The orange represents the magnetization along −x axis, yellow +x axis, green +y axis, and dark green −y axis.
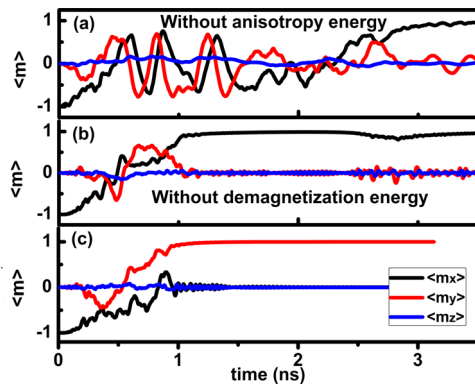
FIG. 5. The temporal magnetization components evolutions of $\langle m_x \rangle$ (black), $\langle m_y \rangle$ (red), and $\langle m_z \rangle$ (blue) at the constant current density of 8.0×10^6 A/cm^2 (a) without taking into account magnetic anisotropy energy, and (b) demagnetization energy (c) with all energies.

formation of magnetic excitations with the wavelength is much shorter than the element size, leading to the formation of multi-domains. If the demagnetization factors of N_x and N_y increase to 0.10, the magnetization switching will show the 90° switching (half switching). Finally, we observe that the magnetization is switched from the initial −x direction to the final +x direction when the demagnetization factors of N_x and N_y increase to 0.20. Thus, we also attribute the elimination of the intermediate state to the increase of the demagnetization factors along x and y axes.

To study the role of magnetic anisotropy and demagnetization energies, we simulated the switching dynamics without the magnetic anisotropy energy E_{ani} and demagnetization energy E_{dem}. Figures 5(a) and 5(b) show the temporal evolutions of $\langle m_x \rangle$ (black), $\langle m_y \rangle$ (red), and $\langle m_z \rangle$ (blue) at the constant current density of 8.0×10^6 A/cm^2 without taking into account magnetic anisotropy and demagnetization energies. Figure 5(c) shows the magnetization evolutions at the same current density including all the energetic contributions. We observe 180° magnetization switching in Figures 5(a) and 5(b), and 90° switching in the Figure 5(c). The magnetic anisotropy energy impedes 180° magnetization switching at the beginning of magnetization oscillation. The magnetization switching time is 3.3 ns in Figure 5(a) without the magnetic anisotropy energy, and the switching time decreases significantly to 1.2 ns with the magnetic anisotropy energy. Therefore, the anisotropy energy first impedes, and then accelerates the magnetization reversal after the magnetization component $\langle m_x \rangle$ is equal to 0. Furthermore, the 90° magnetization switching under the current density of 8.0×10^6 A/cm^2 in Figure 5(c) becomes the 180° switching after removing the demagnetization energy in Figure 5(b). We also observe the small magnetization oscillation after the reversal in Figure 5(b), and it indicates that the demagnetization energy makes magnetization oscillation stable in the easy axis.

IV. CONCLUSIONS

We investigated the effects of magnetic anisotropy and demagnetization energies on spin transfer torque switching of a Heusler CFA-based alloy spin-valve nanopillar using micromagnetic simulations. It is demonstrated that the elimination of the intermediate state is resulted from the decease of effective magnetic anisotropy constant. The magnetization switching can be achieved by increasing the demagnetization factors of x and y axes even with a small current density of 1.0×10^4 A/cm^2, which is 100 times smaller than the normal critical current of 10^6–10^8 A/cm^2. Both magnetic anisotropy and demagnetization energies impede 180° magnetization switching, however, the anisotropy energy significantly reduces magnetization switching time and the demagnetization energy stabilizes magnetization oscillation along the easy axis.

[1]L. Berger, Phys. Rev. B **54**(13), 9353 (1996).
[2]J. C. Slonczewski, J. Magn. Magn. Mater. **159**(1–2), L1–L7 (1996).
[3]J. A. Katine, F. J. Albert, R. A. Buhrman, E. B. Myers, and D. C. Ralph, Phys. Rev. Lett. **84**(14), 3149 (2000).
[4]B. Özyilmaz, A. Kent, D. Monsma, J. Sun, M. Rooks, and R. Koch, Phys. Rev. Lett. **91**(6), 067203 (2003).
[5]E. B. Myers, Science **285**(5429), 867–870 (1999).
[6]M. Tsoi, A. G. M. Jansen, J. Bass, W. C. Chiang, M. Seck, V. Tsoi, and P. Wyder, Phys. Rev. Lett. **80**(19), 4281 (1998).
[7]S. I. Kiselev, J. C. Sankey, I. N. Krivorotov, N. C. Emley, R. J. Schoelkopf, R. A. Buhrman, and D. C. Ralph, Nature **425**(6956), 380–383 (2003).
[8]Y. Jiang, T. Nozaki, S. Abe, T. Ochiai, A. Hirohata, N. Tezuka, and K. Inomata, Nature Mater. **3**(6), 361–364 (2004).
[9]P. M. Braganca, I. N. Krivorotov, O. Ozatay, A. G. F. Garcia, N. C. Emley, J. C. Sankey, D. C. Ralph, and R. A. Buhrman, Appl. Phys. Lett. **87**(11), 112507 (2005).
[10]C.-T. Yen, W.-C. Chen, D.-Y. Wang, Y.-J. Lee, C.-T. Shen, S.-Y. Yang, C.-H. Tsai, C.-C. Hung, K.-H. Shen, M.-J. Tsai, and M.-J. Kao, Appl. Phys. Lett. **93**(9), 092504 (2008).
[11]H. Kubota, A. Fukushima, K. Yakushiji, S. Yakata, S. Yuasa, K. Ando, M. Ogane, Y. Ando, and T. Miyazaki, J. Appl. Phys. **105**(7), 07D117 (2009).
[12]L. Q. Liu, T. Moriyama, D. C. Ralph, and R. A. Buhrman, Appl. Phys. Lett. **94**(12), 122508 (2009).
[13]S. Mitani, J. Phys. D: Appl. Phys. **44**(38), 384003 (2011).
[14]T. Seki, H. Tomita, A. A. Tulapurkar, M. Shiraishi, T. Shinjo, and Y. Suzuki, Appl. Phys. Lett. **94**(21), 212505 (2009).
[15]R. Matsumoto, A. Fukushima, K. Yakushiji, S. Yakata, T. Nagahama, H. Kubota, T. Katayama, Y. Suzuki, K. Ando, B. Georges, V. Cros, J. Grollier, and A. Fert, Phys. Rev. B **80**(17), 174405 (2009).
[16]Z. H. Xiao, X. Q. Ma, P. P. Wu, J. X. Zhang, L. Q. Chen, and S. Q. Shi, J. Appl. Phys. **102**(9), 093907 (2007).
[17]J. Grollier, V. Cros, A. Hamzic, J. M. George, H. Jaffrès, A. Fert, G. Faini, J. Ben Youssef, and H. Legall, Appl. Phys. Lett. **78**(23), 3663 (2001).
[18]G. Finocchio, M. Carpentieri, B. Azzerboni, L. Torres, L. Lopezdiaz, and E. Martinez, Physica B **372**(1–2), 294–298 (2006).
[19]J. C. Lee, C. Y. You, S. B. Choe, K. J. Lee, and K. H. Shin, *IEEE Nanotechnology Materials and Devices Conference*, 604–605 (2006).
[20]G. Finocchio, G. Consolo, M. Carpentieri, A. Romeo, B. Azzerboni, and L. Torres, J. Appl. Phys. **101**(9), 09A508 (2007).
[21]N. C. Emley, I. N. Krivorotov, O. Ozatay, A. G. F. Garcia, J. C. Sankey, D. C. Ralph, and R. A. Buhrman, Phys. Rev. Lett. **96**(24), 247204 (2006).
[22]G. Consolo, G. Finocchio, L. Torres, M. Carpentieri, L. Lopez-Diaz, and B. Azzerboni, J. Magn. Magn. Mater. **316**(2), 492–495 (2007).

[23]V. Bonanni, D. Bisero, P. Vavassori, G. Gubbiotti, M. Madami, A. O. Adeyeye, S. Goolaup, N. Singh, T. Ono, and C. Spezzani, J. Magn. Magn. Mater. **321**(19), 3038–3041 (2009).

[24]T. Aoki, Y. Ando, D. Watanabe, M. Oogane, and T. Miyazaki, J. Appl. Phys. **103**(10), 103911 (2008).

[25]S. Yakata, H. Kubota, Y. Suzuki, K. Yakushiji, A. Fukushima, S. Yuasa, and K. Ando, J. Appl. Phys. **105**(7), 07D131 (2009).

[26]T. Wada, T. Yamane, T. Seki, T. Nozaki, Y. Suzuki, H. Kubota, A. Fukushima, S. Yuasa, H. Maehara, Y. Nagamine, K. Tsunekawa, D. D. Djayaprawira, and N. Watanabe, Phys. Rev. B **81**(10), 104410 (2010).

[27]H. Meng, R. Sbiaa, S. Y. H. Lua, C. C. Wang, M. A. K. Akhtar, S. K. Wong, P. Luo, C. J. P. Carlberg, and K. S. A. Ang, J. Phys. D: Appl. Phys. **44**(40), 405001 (2011).

[28]K. Aoshima, N. Funabashi, K. Machida, Y. Miyamoto, K. Kuga, and N. Kawamura, J. Magn. Magn. Mater. **310**(2), 2018–2019 (2007).

[29]H. Sukegawa, S. Kasai, T. Furubayashi, S. Mitani, and K. Inomata, Appl. Phys. Lett. **96**(4), 042508 (2010).

[30]H. B. Huang, X. Q. Ma, Z. H. Liu, F. Y. Meng, Z. H. Xiao, P. P. Wu, S. Q. Shi, and L. Q. Chen, J. Appl. Phys. **110**(3), 033913 (2011).

[31]H. B. Huang, X. Q. Ma, Z. H. Liu, C. P. Zhao, S. Q. Shi, and L. Q. Chen, Appl. Phys. Lett. **102**(4), 042405 (2013).

[32]H. Sukegawa, Z. Wen, K. Kondou, S. Kasai, S. Mitani, and K. Inomata, Appl. Phys. Lett. **100**(18), 182403 (2012).

[33]H. Huang, X. Ma, Z. Liu, C. Zhao, and L. Chen, AIP Adv. **3**(3), 032132 (2013).

[34]H. Huang, X. Ma, T. Yue, Z. Xiao, S. Shi, and L. Chen, Sci. China: Phys., Mech. Astron. **54**(7), 1227–1234 (2011).

[35]H. B. Huang, X. Q. Ma, Z. H. Liu, F. Y. Meng, S. Q. Shi, and L. Q. Chen, J. Magn. Magn. Mater. **330**, 16–20 (2013).

[36]H. B. Huang, X. Q. Ma, Z. H. Liu, and L. Q. Chen, J. Alloys Compd. **597**, 230–235 (2014).